Experimental and computational study of gas flow delivered by a rectangular microchannels leak

Experimental and computational study of gas flow delivered by a rectangular microchannels leak

M. Bergoglio[1], D.Mari[1], J. Chen[2], H. Si Hadj Mohand[2], S. Colin[2], C. Barrot[2]

1. Istituto Nazionale della Ricerca Metrologica (INRIM), Strada delle Cacce 91, 10135 Torino, Italy

2. Université de Toulouse; ICA (Institut Clément Ader), 1 rue Caroline Aigle, 31400 Toulouse, France

Email of corresponding author: d.mari@inrim.it

Abstract

The gas flowrate through a rectangular microchannels device has been investigated within a collaboration between the Istituto Nazionale di Ricerca Metrologica from Torino and the Institut Clément Ader (ICA) from the University of Toulouse.

The microdevice was characterized with different gas species as He, N_2, Ar, R12, CO_2 and a mixture N_2/H_2 (95/5), in a wide range of pressure, to test its potential use as secondary gas flow standard in terms of ease of use and predictability of gas flowrate.

The measurements of gas flowrates have been carried out in an inlet pressure range between 50 Pa to 100 kPa and with two different outlet conditions: vacuum (10^{-6} Pa up to a few Pa according to the setup) and atmospheric pressure. Furthermore the temperature coefficient has been determined from measurements in a temperature range from 15 °C to 25 °C.

The primary standards of both laboratories were compared and a semi-analytical model was used to predict the molar gas flowrate through the rectangular microchannels in the slip flow and early transition regimes.

Keywords

Micro flowrates; rectangular microchannels; secondary standard leaks; slip flow; transition flow.

1. Introduction

In the framework of the European project EMRP-JRP-IND12 "Vacuum metrology for industrial environments", the experimental and theoretical study of small gas flows has been approached because of its crucial importance in many branches of industry (cold storage facilities, air conditioning systems whose leak rates have to follow the rules of e.g.

DIN 8964 and EN 14091, containment systems for toxic, radioactive and environment polluting substances). The most sensitive, versatile and accurate method for leak measurement is the permanent gas (helium) flowrate measurement through the leak into vacuum. Nevertheless, the leaks usually occur under conditions different from those at measurement: different pressures, temperature and temperature gradients, gas species and mixtures. Research is needed to provide industry with traceability under practical conditions and enabling users of calibrated leaks to predict leak rates under industrial environments [1, 2].

Within the framework outlined by EMRP-JRP-IND12, in order to meet this requirement, cooperation between the Istituto Nazionale di Ricerca Metrologica (INRIM) from Torino and the Institut Clément Ader (ICA) from the University of Toulouse allowed to consider a microdevice with well-defined geometry. The microdevice, encased in a suitable box to maintain constant temperature, was characterized by the primary standards of both laboratories with different gas species, obtaining calibration curves referred to atmosphere and to vacuum in a wide inlet pressure range.

Afterwards a semi-analytical model was used to predict the molar gas flowrate through the rectangular microchannels in the slip flow and early transition regimes and the results were compared with experimental data.

In addition , the study presented in the paper allowed to test the use of the microdevice as secondary gas flow standard for industrial purpose: the gas flow delivered by the device can be estimated through the developed semi-analytical model, without carrying out several measurements for each gas and in a wide range of inlet pressure.

2. Microsystem leak device

The microsystem T4P leak device consists in a series of parallel rectangular microchannels etched by deep reaction ion etching (DRIE) on a 4 inches diameter silicon wafer and closed by anodic bonding with a 3 inches diameter Pyrex plate.

The characteristics of the microchannels are listed in table 1. The 575 rectangular cross-section channels with an aspect ratio $a^* = H / W$ equal to 0.0109 are connected to 300 µm deep upstream and downstream reservoirs as shown in figure 1.

Microchannels	**Depth, *H* (µm)**	**Width, *W* (µm)**	**Length, *L* (µm)**	**Number of microchannels, *n***
Value	0.53	50.0	5000	5×115=575
Uncertainty	0.01	0.3	10	

Table1. Microsystem T4P specifications

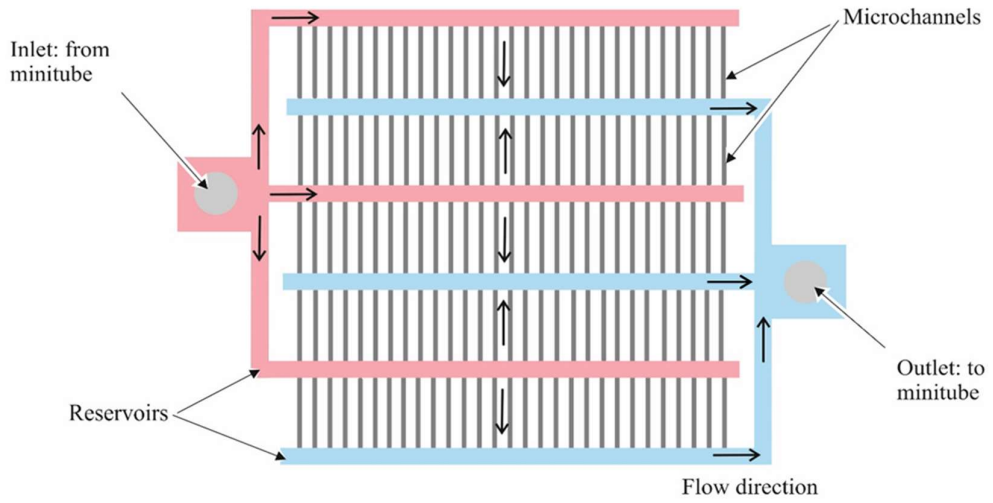

Figure 1. Schematic of microsystem T4P

The depth and the roughness have been measured with a TENCOR P1 profilometer, obtaining a depth of 0.53 µm with a standard uncertainty of 0.01 µm.

The typical roughness at the bottom of the channels has been estimated between 50×10^{-10} m and 80×10^{-10} m. The width has been determined by an optical microscope with an uncertainty of 0.3 µm. The microchannels length which corresponds to the distance between the branches of the reservoirs has been directly deduced from the mask dimension known with an uncertainty of 10 µm. All details on the measurement of these lengths are presented in [3].

3. Experimental setups and procedures

The measurements have been focused on three objectives:

1) Characterization of the microsystem with different gas species in a wide inlet pressure range, from 50 Pa to 100 kPa and with two different outlet conditions: vacuum (10^{-6} Pa up to a few Pa according to the setup) and atmospheric pressure.

2) Comparison of standards developed at INRIM and ICA laboratories.

3) Measurements of gas flowrate in a temperature range from 15 °C to 25 °C to determine the temperature coefficient.

3.1 INRIM experimental setup

The quantity generated by the device and measured by a primary standard flowmeter is the molar gas flowrate, defined as the number of gas moles coming out from the device per unit of time.

Two INRIM primary standard flowmeters, based on constant-pressure and variable-volume method, were used. The first one measures the molar flowrate under atmospheric pressure

condition in the range 4×10^{-10} mol/s to 2×10^{-7} mol/s with reference to atmospheric pressure [4]; the second flowmeter generates and measures gas flowrates between 4×10^{-12} mol/s and 4×10^{-7} mol/s against vacuum [5].

INRIM primary flowmeters participated successfully to an International Comparison [6] and an Euramet TC-M Project [7], in accordance with the Mutual Recognition Arrangement.

3.1.1 Setup referred to atmosphere

Measurement System

Figure 2 shows the schematic of the system. The reference and measurement volumes V_R and V_M are maintained at the same reference atmospheric pressure p_{atm}. After the closing of valve V2, valve V3 is closed and the capacitance diaphragm gauge CDG (133 Pa full scale) measures the differential pressure between the two volumes V_R and V_M. Afterwards, valve V4 is opened to the flowmeter and the gas from T4P flows to the measurement volume V_M, increasing the pressure inside it. The pressure variation is compensated by a volume decreasing carried out by a piston-bellows coupling.The pressure variation is controlled between two thresholds by the reading of CDG: when the pressure inside V_M exceeds the upper threshold, the piston-bellows coupling moves to perform a volume variation ΔV to decrease the pressure to a value less than the lower threshold. The process is repeated several times, obtaining a saw-tooth variation of differential pressure between the two volumes; the differential pressure decreasing corresponds to a movement of the piston-bellows coupling.

The temperatures of V_R and V_M are measured and monitored by PT100 devices during each measurement.

The molar gas flowrate q from T4P can be expressed by the following approximated formula:

$$q \cong \frac{p_{atm}}{RT_M}\frac{\Delta V_M}{\Delta t} \qquad (1)$$

where R is the universal gas constant, T_M the temperature in the volume V_M, ΔV_M the volume variation carried out by the piston-bellows system and Δt is the time difference between two points at the same pressure.

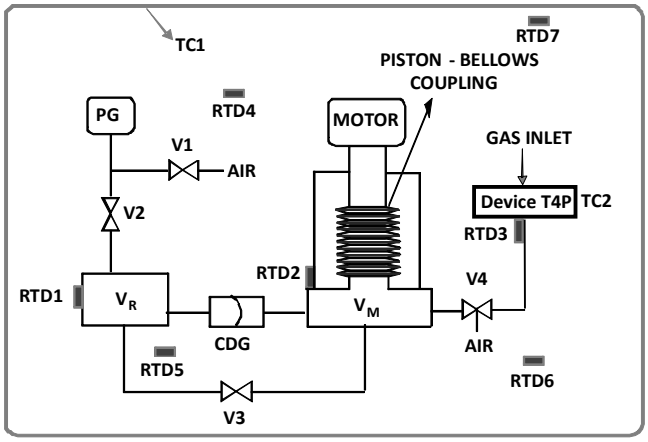

Figure 2. Schematic of primary standard flowmeter. V_R and V_M: reference and measurement volumes; TC1 and TC2: thermal control boxes respectively for the whole flowmeter and T4P; RTDs: temperature sensors; CDG: Capacitance Diaphragm Gauge (133 Pa); PG: pressure gauge for reference atmospheric pressure measurement.

An active thermal control is used to control and maintain constant temperature in the whole flowmeter.

Measurement model and uncertainty budget

The model adopted for the determination of molar gas flowrate delivered from T4P is a direct consequence of the application of the ideal gas law.

Under the assumptions that the effects of adsorption and eventual leakage of molecules in V_R and V_M and the variation of the two volumes due to temperature are negligible, the molar gas flowrate at time $t_1 = t_0 + \Delta t$ is given by [4]:

$$q = \frac{p_{atm}}{RT_M} \cdot \frac{\Delta V_M}{\Delta t} + \frac{V_M}{RT_M} \cdot \frac{p_{atm}}{T_R} \frac{\Delta T_R}{\Delta t} - V_M \frac{p_{atm}}{RT_M^2} \cdot \frac{\Delta T_M}{\Delta t} \tag{2}$$

Equation (2) shows that the accuracy of the gas flowrate measurements strongly depends on the temperature stability of the system which has to be monitored.

The global temperature effect on measurement is estimated measuring the pressure drift registered by CDG after the closing of valve V3 (volume V_R and V_M are separated), before introducing the gas (released by the leak device T4P) inside the measurement volume. The drift is estimated by least squares method, obtaining the slope m_c related to temperature influence, fitting the differential pressure from CDG versus time.

As a consequence, the measurand is given by the following equation, which represents the final model used for the calculation of gas flowrate and its standard uncertainty:

$$q = \frac{1}{h}\sum_{i=1}^{h}\left[\frac{1}{RT_{M,i}} p_{atm} \pi \frac{D^2}{4} \Delta L_i \Big/ \left(\frac{n_i}{m_i - m_c} - \frac{n_{i+1}}{m_{i+1} - m_c}\right)\right] = \frac{1}{h}\sum_{i=1}^{h}\left[\frac{1}{RT_{M,i}} p_{atm} \frac{\Delta V_{M,i}}{\Delta t_i}\right] \tag{3}$$

where the index i is related to each pressure rise associated to the saw-tooth variation of

differential pressure between the reference and measurement volume of the flowmeter [4]; h is the number of pressure rises, D is the piston diameter, ΔL_i the displacement variation carried out to decrease the reading of CDG to a value less than the lower threshold, m_i and n_i respectively the slope and the intercept for each pressure rise, estimated by a least squares linear fit and m_c the correction related to temperature effect.
Equation (3) expresses the relationship between the measurand (the output quantity q) and the input quantities and it can be used to evaluate the standard uncertainty of gas flowrate q [8, 9, 10] starting from the standard uncertainty of each input quantity.

The reference atmospheric pressure p_{atm} is measured by a MKS Baratron CDG (133 kPa full scale), which is periodically calibrated with INRIM interferometric mercury manometer. The relative standard uncertainty $u(p_{atm})/p_{\mathrm{atm}}$ was evaluated as 8.0×10^{-4}.

The geometrical characterization of piston was performed at INRIM [11]. The relative standard uncertainty of its diameter $u(D)/D$ is 3.6×10^{-4}.

The measurement of piston displacement is determined by a stepping-motor. The uncertainty $u(\Delta L)$ depends substantially on resolution and repeatability of stepping motor drive. It was characterized by a Michelson interferometer, obtaining a standard uncertainty $u(\Delta L)= 1.2\times10^{-6}$ m.

The parameters m_c, m_i and n_i are estimated by linear regression of pressure versus time. The time measurements are performed by the PC internal clock, which is traceable to INRIM atomic clock. The relative standard uncertainty of time difference $\Delta t=n_i/(m_i- m_c)-n_{i+1}/(m_{i+1}- m_c)$ is less than 8.0×10^{-4}.
The temperature of the measurement volume of the flowmeter has been measured by a temperature sensor traced to International Temperature Scale (ITS-90) at INRIM. The relative standard uncertainty of temperature is 3.4×10^{-4}.

Type A uncertainty, which is not only due to the primary system, but depends also on stability of standard leak under calibration, is revealed in the scatter of repeated calibrations. It is obtained considering the experimental standard deviation of the mean value of the molar gas flowrate. In the worst case, the relative type A standard uncertainty is 2.2×10^{-2}.

The combined relative standard uncertainties range from 4.6×10^{-2} to 0.4×10^{-2} between 4×10^{-10} mol/s and 2×10^{-7} mol/s.

3.1.2 Vacuum setup

Measurement System

The flowmeter can generate and measure molar flowrate in the range between 10^{-12} mol/s and 10^{-7} mol/s. The gas flow is generated by gas leaking out from the measurement volume V_M (figure 3) through the device T4P under calibration. The initial reference pressure p_{ref} (from 10 Pa to 10^5 Pa) is measured by a set of CDGs.The decrease of pressure due to the gas leak is compensated by a volume variation in V_M, applied through two pistons (5 mm and 20 mm diameter), that are moved by two motors.

The descent speed of the chosen piston is regulated by an electronic servo system in order to maintain a constant (usually in the range 10^{-3} Pa to 10^{-2} Pa) zero signal associated to the differential pressure between V_R and V_M , measured by CDG1.

The throughput q_{pV} is given by:

$$q_{pV} = RT\frac{dN}{dt} = \frac{d(p_{ref}V_M)}{dt} = p_{ref}\frac{dV_M}{dt} = p_{ref}\pi\frac{D^2}{4}\frac{dL}{dt};\ \frac{dT}{dt} = 0;\ \frac{dp_{ref}}{dt} = 0 \qquad (4)$$

where D and L are respectively the diameter and the displacement of the chosen piston.

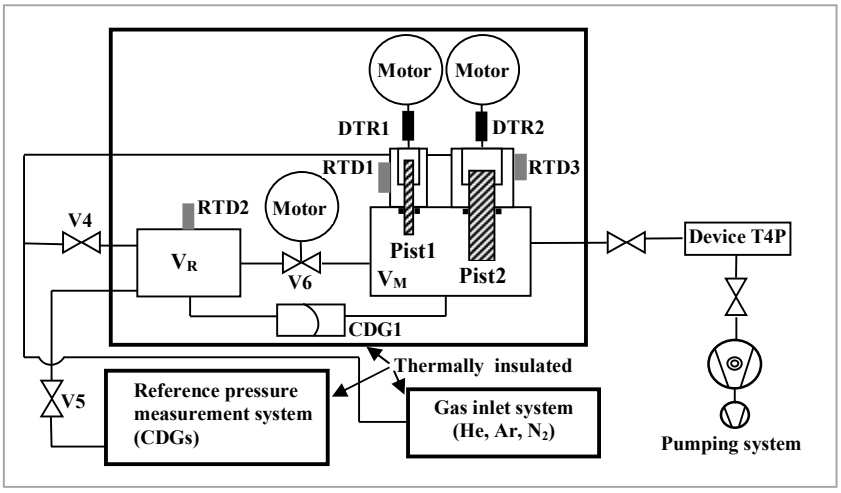

Figure 3. Schematic of the INRIM primary flowmeter. V_R and V_M: reference and measurement volumes; CDG: Capacitance Diaphragm Gauge (133 Pa); RTDs: temperature sensors; DTRs: displacement transducers

Measurement model and uncertainty budget

The model equation is given in (4). The CDGs used to measure the reference pressure p_{ref} are calibrated against the INRIM interferometer mercury manometer and against the static expansion system; $u(p_{ref})$ is due to calibration uncertainty, resolution, stability of the gauge and repeatability of data acquisition during each measurement. The component due to the residual pressure in the flowmeter is negligible. $u(p_{ref})/p_{\mathrm{ref}}$ was evaluated as 2.0×10^{-3}.

The dimensional characterization of the pistons was carried out at INRIM. The averages of radii values obtained on a direction were used to calculate the piston area A; $u(A)/A$ is 1.2×10^{-3} for piston 1 and 3.0×10^{-4} for piston 2.

The descent speed of the piston dL/dt was determined by fitting the displacement of the chosen piston versus time. A linear regression was applied in accordance with Gauss-Markov theorem. The relative standard uncertainty of descent speed ranges from $.0\times10^{-4}$ to 2.3×10^{-3}. It was evaluated considering the components due to calibration of displacement transducers and mathematical model. The component of uncertainty due to time measurements was considered negligible.

Equation (4) is based on the hypothesis that both the reference pressure and the temperature are maintained constant during measurements. The deviations from these ideal conditions was investigated and considered in the uncertainty budget. The relative standard uncertainty, due to this term, ranges from 9.3×10^{-3} to 1.1×10^{-4}.

The contribution due to the repeatability of gas flowrate measurements was also considered: it is significant in the lower range where, in the worst case, at 1×10^{-8} Pa m^3 /s, its value is 2.2×10^{-2}. The combined relative standard uncertainty ranges from 2.6×10^{-2} to 2.9×10^{-3} between 4×10^{-12} mol/s and 4×10^{-7} mol/s.

3.2 ICA experimental setup

Measurement System

The experimental setup developed at ICA [12, 13], is shown in figure 4

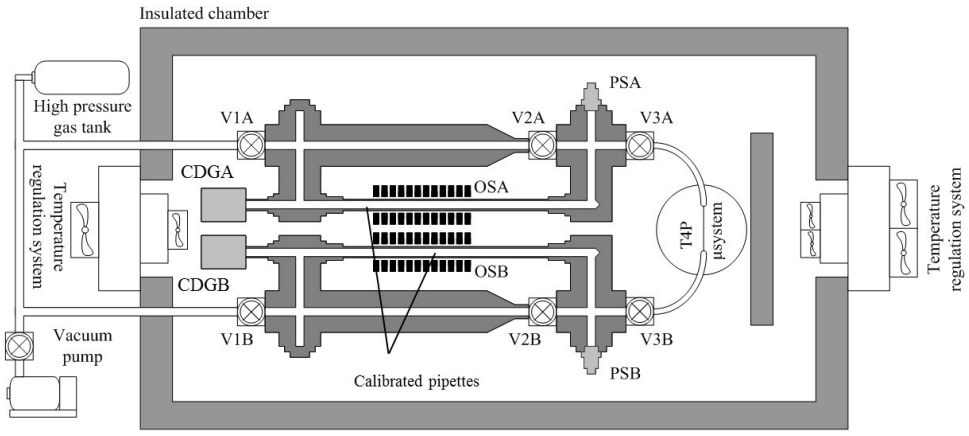

Figure 4. Diagram of the ICA experimental setup (electrical wiring, temperature sensors and data acquisition system are not shown)

The microsystem leakdeviceT4P is connected via valve V3A to the upstream circuit A and via valve V3B to the downstream circuit B. If necessary, the role of circuits A and B may be inverted, B becoming the upstream circuit. Each circuit A (resp. B) includes three valves, V1A, V2A and V3A (resp. V1B, V2B and V3B), one calibrated pipette–into which a liquid drop has been previously inserted–equipped with opto-electrical sensors OSA (resp. OSB), one Kulite piezoresistive pressure sensor PSA (resp. PSB), and one Inficon high-sensitivity capacitance diaphragm gauge CDGA (resp. CDGB).

The setup can operate with pressures ranging from 10 Pa to 1.3×10^5 Pa. The flow of gas is generated by a pressure difference imposed between the inlet and the outlet of microsystem T4P.

All ICA measurements presented in this paper have been obtained using the Constant Volume (CV) method.

The pressure variations are accurately monitored and measured by means of two kinds of pressure sensors in function of the levels of pressure at the inlet and outlet: three Inficon CDGs (full scale 133 kPa, 13.3 kPa, 1.33 kPa) and piezoresistive Kulite sensors (full scale 350 kPa).

The temperature is a crucial quantity; for that purpose, two Peltier modules associated to several fans control the temperature inside the insulated chamber. Three sensors (PT100) are continuously used to monitor the temperature. Two of them are placed on the reservoirs shields and the third one is placed in the vicinity of microsystem T4P.

For all the experiments presented in this section, the temperature was regulated at a nominal value of 20 °C.

Measurement model and uncertainty budget

In CV method, the mass flowrate calculation is deduced from the ideal gas equation of state applied to the volume of gas in circuits A and B:

$$\frac{dM_{A,B}}{dt} = \frac{d}{dt}\left(\frac{pV}{R_g T}\right)_{A,B} \tag{5}$$

where R_g is the specific gas constant, $M_{A,B}$ is the mass of gas in circuits A or B with a volume $V_{A,B}$, a pressure $p_{A,B}$ and a temperature $T_{A,B}$. The mass flowrate through microsystem T4P is then obtained from:

$$\dot{M}_{A,B} = \frac{V_{A,B}}{R_g T_{A,B}} \frac{dp_{A,B}}{dt}\left(1 - \frac{dT/T}{dp/p}\right)_{A,B} \tag{6}$$

The standard deviation of the temperature is in all cases around 0.1 K. The relative temperature variation $\Delta T / T$ is then of the order of 4×10^{-4}, to be compared with the relative pressure variation $\Delta p / p$ of the order of 2×10^{-2}. As a consequence, equation (6) can be approximated by:

$$\dot{M}_{A,B} = \frac{V_{A,B}}{R_g T} a_{A,B}\, c_{A,B} \tag{7}$$

where $a = \Delta p / \Delta t$ is calculated in each circuit from a least-square linear fit of the measured pressure

$$p(t) = at + b \tag{8}$$

and $c = 1 - \dfrac{\Delta T / T}{\Delta p / p}$.

More than 1000 pressure data are used for determining coefficients *a* and *b*. The standard deviation of coefficients *a* is calculated following the method proposed in [14].

Outgassing and small leakages from the setup when operating at low pressure could sometimes occur and could not be neglected, and consequently must be taken into account to correct the flowrate data [12].

The volumes of circuits A and B have been accurately measured with a specific setup [12].

The relative standard uncertainty of the volume for circuit A (or B) has been calculated as 7.7×10^{-3}, in accordance with [10].

The relative standard uncertainty of temperature has been evaluated equal to $2.8\times10^{-3}$and finally the relative standard uncertainties $u(c)$ and $u(a)$ are respectively 4.0×10^{-3} and 5.4×10^{-3}.

The mass flowrate uncertainty has been calculated taking into account the standard uncertainty of the input quantities of model equation (7): the relative combined uncertainty associated to mass flowrate is equal to 4.0×10^{-2}, taking into account the component due to outgassing and leakages.

4. Analysis of results

The rarefaction parameter δ is defined at the inlet (*i*) and at the outlet (*o*) of T4P as

$$\delta_{i,o} = H \frac{p_{i,o}}{\mu\sqrt{2R_g T}} \tag{9}$$

where *H* is the depth of the channel, p the pressure and μ the dynamic viscosity of the gas at the temperature T of the experiment; δ_0 represents the mean value:

$$\delta_0 = \frac{\delta_i + \delta_o}{2} \tag{10}$$

The mean Knudsen number Kn_0 is then defined as:

$$Kn_0 = \frac{\sqrt{\pi}}{2\delta_0} \tag{11}$$

The reduced flowrate G^* is deduced from the mass flowrate $\dot{M}$ according to:

$$G^* = \dot{M}\sqrt{2R_g T}\,\frac{L}{nW\,H\,D_h(p_i - p_o)} \tag{12}$$

where the hydraulic diameter is $D_h = 4\,S / P_w$, with S representing the cross-section area and P_w the wetted perimeter of the microchannels.

4.1 INRIM measurements

T4P device was installed in horizontal position and maintained at the temperature of (20.0 ± 0.30) °C; to control the temperature of the device, an aluminium case with channel for water circulation was realized and connected to an external water bath.

The results of the measurements carried out for the considered gases are shown in figure 5 in terms of reduced flowrate G^* vs Kn_0; the complete data set is reported in appendix.

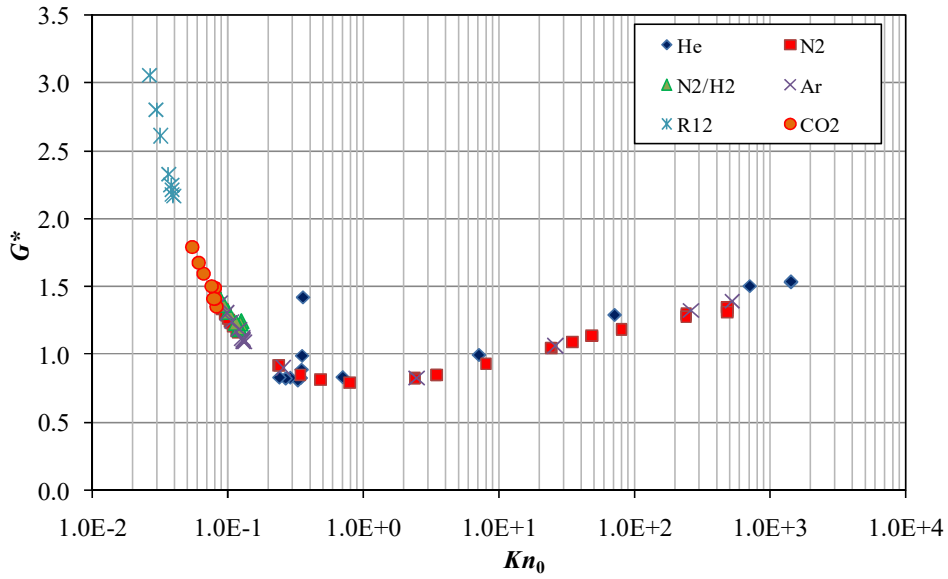

Figure 5. Reduced flowrate G^* vs Kn_0 – INRIM setup

The measurements carried out with helium, flowing to the atmosphere, show an anomalous deviation from the general tendency for Kn_0= 0.5, which is not expected; to avoid the doubt

of eventual experimental mistakes, the measurements have been repeated two months after: the results have shown a very good repeatability compared with the previous one, confirming the anomalous results only in case of helium.

The measurements carried out with reference to vacuum have shown a reduced flowrate which is not constant for all the considered gases (helium, nitrogen, argon) also in case of Knudsen number greater than 10, where a molecular regime is expected. The unusual detected effect is probably related to the device, in fact in the framework of EMRP IND12, several measurements have been performed with different kind of leaks: in all the cases, the results, at low inlet pressures, highlight the typical behaviour of molecular regime, confirming that the flowmeter works properly [15].

4.2 ICA measurements

The experimental data obtained for argon, nitrogen and carbon dioxide are presented in figure 6.

The mass flowrates $\dot{M}_A$ and $\dot{M}_B$ have been measured upstream and downstream from T4P, except when the downstream circuit was connected to the vacuum pump. The mass flowrate $\dot{M} = (\dot{M}_A + \dot{M}_B)/2$ has been used for calculating the reduced flowrate G^* with equation (12).

A summary of all the experiments made at ICA is presented in figure 6; the complete data set is reported in appendix.

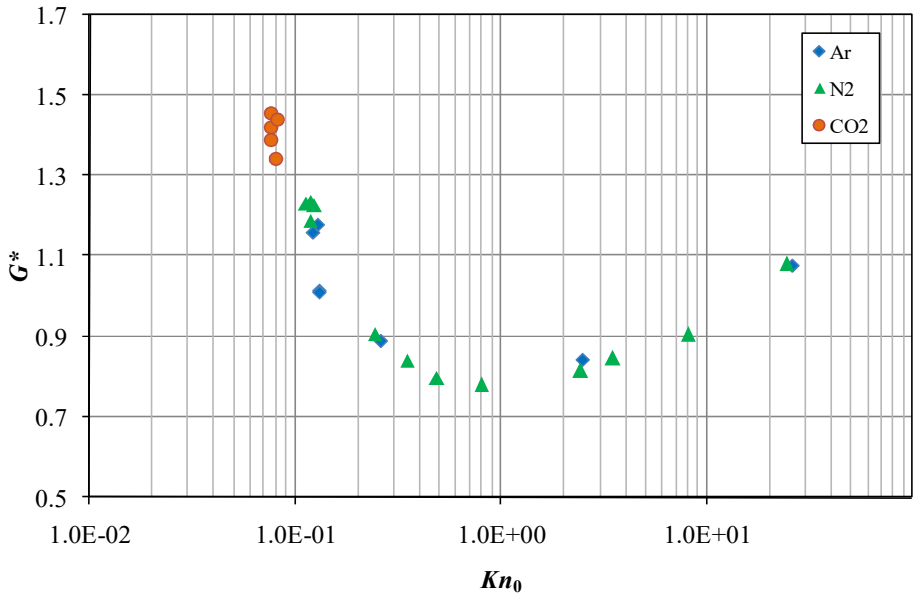

Figure 6. Reduced flowrate G^* vs Kn_0 – ICA setup

4.3 Comparison between INRIM and ICA standards

The respective standards of INRIM and ICA laboratories have been compared to test their equivalence.

Argon and nitrogen were considered, performing the measurements in the same conditions. Experimental conditions of each gas, the molar flow and its standard uncertainty for both laboratories are tabulated in the appendix.

4.3.1 Evaluation of the reference value as weighted mean

As mentioned in the guide [8] of the BIPM Director's Advisory Group on Uncertainties, the weighted mean has been used as estimator of reference value. This procedure can be applied because each laboratory assigns a Gaussian probability distribution function to the measurand. The weighted mean value q_w was determined by using the general Gauss-Markov theorem and considered as reference value of the comparison.

The value of the degree of equivalence [9] for each participant with respect to the reference value, is determined from the difference $d_j = q_{lab,j} - q_{ref,j}$ and its associated uncertainty, which is given by:

$$u(d_j) = \sqrt{u^2(q_{lab,j}) - u^2(q_{ref,j})} \tag{13}$$

where index j is related to the measurement point, $q_{ref,j}$ is the reference value of molar gas flowrate and $q_{lab,j}$ the value referred to each laboratory.

4.3.2 Results of the comparison

The following results are related to data obtained with a very close inlet-outlet pressure difference Δp. Figures 7 and 8 show the difference *d and its* expanded ($k = 2$) uncertainty *U(d)* for each nominal Δp (inlet-outlet).

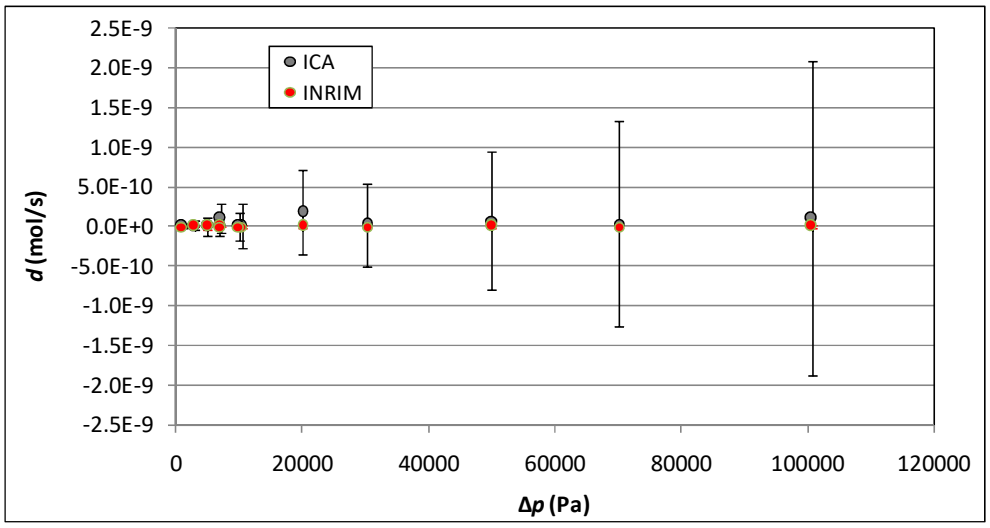

Figure 7. INRIM and ICA comparison results: difference of experimental and reference values versus delta *p*; for each point, the uncertainty of the difference is shown - Nitrogen

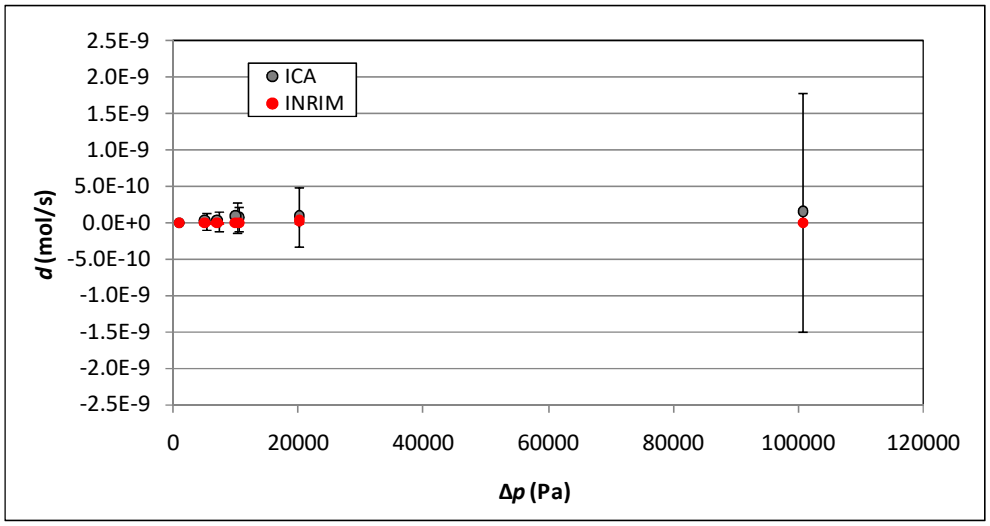

Figure 8. INRIM and ICA comparison results: difference of experimental and reference values versus delta *p*; for each point, the uncertainty of the difference is shown - Argon

The results presented in the previous figures show that the ratio between the difference *d* and its expanded uncertainty is always lower than one, i.e. the full equivalence of both standards is proved.

4.4 Temperature coefficient of the micro-device

A study of temperature dependence of device was carried out with nitrogen, with the assumption of linear model in the considered range between 15 °C and 30 °C:

$q_T = q_{T_0}(1 + \alpha\Delta T)$; $\Delta T = (T - 20)$ °C

where q_T is the gas flowrate measured at the temperature T , q_{T_0} the gas flowrate at the reference temperature of 20 °C and α is the temperature coefficient.

The study has been performed with the aim to compare the temperature dependence characterization of the microsystem T4P with the previous results of temperature coefficient related to different kinds of leaks, obtained in the framework of EMRP-IND12.

The temperature coefficient for nitrogen has been estimated by least squares method, obtaining the following value:

$\alpha_{Nitrogen}$= (- 0.00215 ± 0.00015) °C^{-1}

The temperature coefficient shows a negative value confirming, as in the case of other leaks previously studied in the framework of the project EMRP-JRP-IND12, that the gas flow released by the device is dependent on viscosity.

Furthermore , the measured value of temperature coefficient of the rectangular microdevice is similar to the values founded in case of metal crimped capillary, glass capillary and micro-holes in metal material, studied in EMRP-JRP-IND12, confirming that, for the microdevice T4P, the temperature is not critical in the considered range.

5. Theoretical Model

The experiments conducted in this work are covering two flow regimes. The first one is the transition regime, with high Knudsen numbers (roughly between 10^{-1} and 10^{+3}). For this regime, the theoretical solutions can only be obtained by numerical resolution of kinetic model equations.

The second one is the slip flow regime, for Knudsen numbers between 10^{-2} and 10^{-1}. In this regime, an analytical solution, based on the compressible Navier-Stokes equations associated with velocity-slip and temperature-jump boundary conditions, can be derived. Although first order boundary conditions can be accurate enough [16] for low values of *Kn*, for higher values of *Kn*, the accuracy should be improved using second-order boundary conditions. In this paper, the experimental data are compared with a semi-analytical model of flow in rectangular microchannel based on second-order boundary conditions similar to those developed by Deissler [17] and further improved by Pitakarnnop et al [12]. These conditions take the form:

$$v\big|_{x=\pm\frac{W}{2}} = \mp A_1\lambda \left.\frac{\partial v}{\partial x}\right|_{x=\pm\frac{W}{2}} + A_2\lambda^2 \left.\left(\frac{\partial^2 v}{\partial x^2} + B_2\frac{\partial^2 v}{\partial y^2}\right)\right|_{x=\pm\frac{W}{2}}$$

$$v\big|_{y=\pm\frac{H}{2}} = \mp A_1\lambda \left.\frac{\partial v}{\partial y}\right|_{y=\pm\frac{H}{2}} + A_2\lambda^2 \left.\left(\frac{\partial^2 v}{\partial y^2} + B_2\frac{\partial^2 v}{\partial x^2}\right)\right|_{y=\pm\frac{H}{2}}$$

(14)where v is the streamwise velocity and $A_1 = \beta(2-\alpha)/\alpha$ is the first order coefficient, α being the tangential momentum accommodation coefficient. It is here assumed that

$\alpha = 1$, which corresponds to a purely diffuse reflection at the walls. Values of coefficients β, A_2 and B_2 have been proposed by several authors; the references of the main corresponding works can be found in [18]. In this paper, the following coefficients suggested in [12] have been selected: β=1.1466, A_2=-0.647 and B_2 =1/2.

Aubert and Colin [19] proposed a semi-analytical model of the molar flowrate in rectangular microchannels using Deissler boundary conditions, as a function of the pressure ratio $\Pi = p_i / p_o$ and the outlet Knusden number $Kn_o = \sqrt{\pi}/(2\,\delta_o)$:

$$q = n\frac{H^4}{4a^*\mu L}\frac{p_o^2}{RT}\left(\frac{a_1\left(\Pi^2-1\right)}{2} + a_2 Kn_o(\Pi-1) + a_3 Kn_o^2 \ln\Pi\right) \tag{15}$$

The coefficients a_1, a_2 and a_3 depend on the aspect ratio $a^* = H/W$ and on the accommodation coefficient α. For $a^* = 0.0106$ and $\alpha = 1$, the model developed in [19] with the above values of β, A_2 and B_2 leads to the following coefficients: $a_1 = 0.33111$, $a_2 = 2.1581$ and $a_3 = 2.7289$.

The relative deviation between theoretical and experimental values of molar flowrate are reported in figures 9 and 10, as a function of the mean Knudsen number Kn_0. A good agreement with a deviation lower than 10% has been observed for most of the measurements except for a few data for which the relative deviations are systematically lower than 15 % .

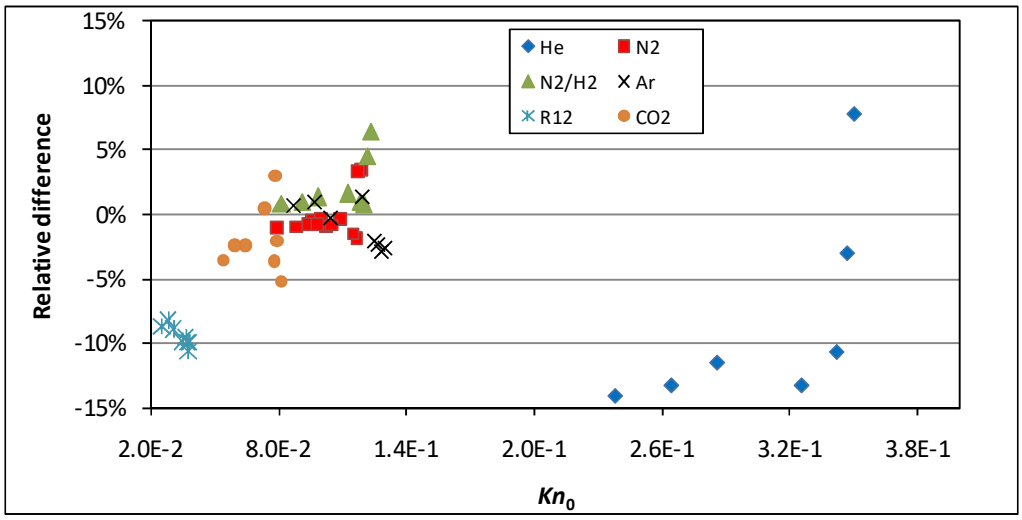

Figure 9. Relative deviation between experimental and theoretical flowrates calculated from equation (16) for several gas species with INRIM setup described in chapter 3.1.

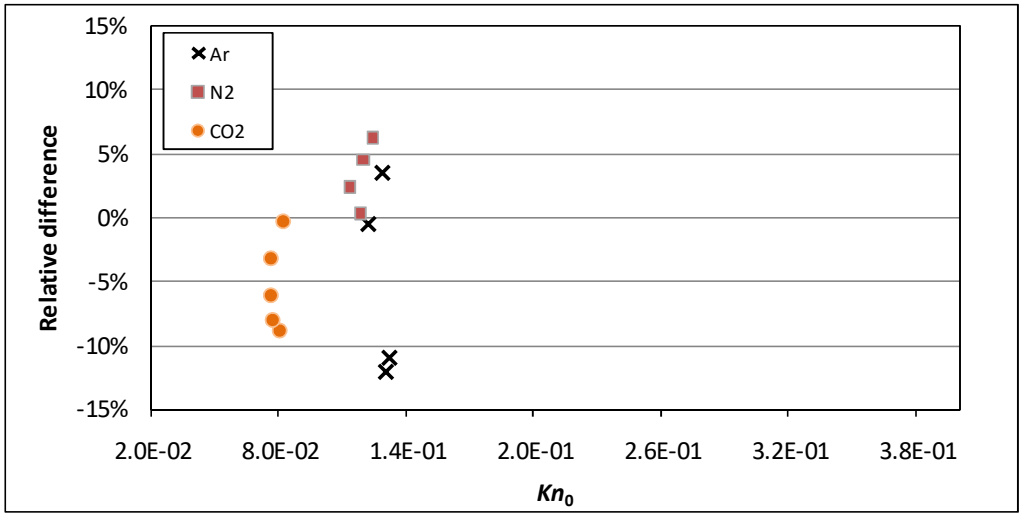

Figure 10. Relative deviation between experimental and theoretical flowrates calculated from equation (16) for different gas species with ICA setup described in chapter 3.2.

6. Conclusions

In the framework of the project EMRP-JRP-IND12 " Vacuum metrology for industrial environments", the experimental and theoretical study of small gas flows has been approached because of its crucial importance in many branches of industry.

In particular, a cooperation between INRIM and Toulouse University started, with the aim to check the possibility to use a micro-multichannel device with well define geometry as secondary standard leak. The micro-device consists of a series of parallel rectangular microchannels, etched by deep reactive ion etching (DRIE) in a silicon wafer and closed by anodic bonding with a Pyrex plate.

For this purpose, as first step, the device was characterized with measurements referred both to vacuum and atmospheric pressure with different gases such as He, N_2, Ar, R12, CO_2, and a mixture N_2/H_2 (95/5) to study the stability and repeatability. Furthermore temperature dependence of the micro-device was investigated to compare the obtained results with the previous data related to different kinds of leaks studied in the framework of EMRP-JRP-IND12: the temperature coefficient shows a negative value confirming, as in the case of other leaks previously studied, that the gas flowrate released by the micro-device is dependent on viscosity.

At the same time a comparison of the INRIM and ICA standards using the micro-device as transfer standards was carried out.

The results of the comparison between the two standards showed a complete equivalence of the standards of the two laboratories involved in the measurements.

Finally a theoretical model of flowrate in the slip flow regime was used to predict the gas flowrate through the micro-device. The results in slip and early transition regime show a

good agreement with the experimental values generally lower than 10% and always lower than 15%.

The deviations can be attributed to specific behaviours of the different gas species, which can exhibit accommodation coefficients slightly different from unity. In Figure 9, the data for He have been obtained in a transitional regime (Kn = 0.24-0.36), while the adopted model is accurate in the slip flow regime (Kn = 0.1-0.01); this can explain the larger deviation of the relative difference between experimental and theoretical results for this gas. In addition, this model should be robust with simple gas, but more complex interactions between polyatomic molecules and the wall can lead to some small deviations. These deviations are globally in accordance with other similar experimental investigations, which underline that more theoretical investigation is still necessary for determining both the more appropriate boundary conditions and the best way to determine the accommodation coefficients.

The device shows a low temperature coefficient in the considered temperature range and a good stability in time, therefore it could be useful as secondary standard leak in the industrial leak testing application.

The presented study also aims to meet the needs of industry in terms of predictability of gas flow from a secondary leak standard, in particular allowing to deduce the refrigerant gas flow delivered by the device, using the semi-analytical model described in the paper and starting only from few calibration points obtained with a simple gas such as nitrogen. The device described in the present paper has a well-known geometry, which allows a better predictability compared to crimped capillaries, which geometry cannot be determined due to the crimping process with which they are manufactured.

Acknowledgement

This work was supported by EMRP IND12 project. The EMRP is co-financed by EMRP participants within EURAMET and the European Union.

The authors wish to thank S. Pasqualin (INRIM) for its fruitful support in the experimental characterization of the microdevice.

References

[1] M. Bergoglio, D. Mari, Leak rate metrology for the society and industry, Measurement 45 (2012), 2434-2440

[2] A. Calcatelli, M. Bergoglio, D. Mari, Leak detection, calibrations and reference flows: Practical example, Vacuum 81,11-12 (2007), 1538-1544

[3] P. Lalonde (2001), Etude expérimentale d'écoulements gazeux dans les microsystèmes à fluides PhD, Institut National des Sciences Appliquées de Toulouse.

[4] M. Bergoglio, D. Mari, INRIM primary standard for microgas-flow measurements with reference to atmospheric pressure, Measurement 45 (2012), 2459-2463
[5] M. Bergoglio, D. Mari, INRIM continuous expansion system as high vacuum primary standard for gas pressure measurements below 9×10^{-2} Pa, Vacuum 84, 1 (2009), 270-273
[6] K Jousten, K Arai, U Becker, O Bodnar, F Boineau, J A Fedchak, V Gorobey, Wu Jian, D Mari, P Mohan, J Setina, B Toman, M Vičar and Yu Hong Yan, Final report of key comparison CCM.P-K12 for very low helium flow rates (leak rates), Metrologia 50 (2013)
[7] International Euramet TC-M Project 911 (2006-2013)
[8] M. G.Cox, The evaluation of key comparison data, Metrologia, 39 (2002), 589-595.
[9] Guideline for CIPM comparison, Appendix F to MRA, March 1999, (http:www.bipm.org).
[10] BIPM, IEC, IFCC, ILAC, ISO, IUPAC, IUPAP and OIML 2008 Evaluation of Measurement Data-Guide to the Expression of Uncertainty in Measurement , JCGM 100 (accessed 16 November 2009).
[11] F. Alasia, A. Calcatelli, G. Cignolo, G. Raiteri, G. Rumiano, IMEKO TC 16 International Symposium on Pressure and Vacuum, Proc. Acta Metrologica Sinica Press, Beijing, China, September 22-24, 2003.
[12] J. Pitakarnnop, , S. Varoutis, D. Valougeorgis, S. Geoffroy, L. Baldas and S. Colin. "A novel experimental setup for gas microflows." Microfluidics and Nanofluidics 8, 1 (2010), 57-72.
[13] Szalmás, L., Pitakarnnop, J., Geoffroy, S., Colin, S., and Valougeorgis, D., Comparative study between computational and experimental results for binary rarefied gas flows through long microchannels, Microfluidics and Nanofluidics, 9, 6 (2010), 1103-1114 10.1007/s10404-010-0631-2.
[14] T. Ewart, , P. Perrier, , I. Graur, , and J. G. Méolans, , Mass flow rate measurements in gas micro flows, Experiments in Fluids, 41, 3 (2006), 487-498.
[15] Ute Becker et al., Realization, characterization and measurements of standard leak artefacts, Measurement 61 (2015), 249-256
[16] S. Colin, , "Rarefaction and compressibility effects on steady and transient gas flows in microchannels." Microfluidics and Nanofluidics 1, 3 (2005), 268-279.
[17] R. G. Deissler, "An analysis of second-order slip flow and temperature-jump boundary conditions for rarefied gases." International Journal of Heat and Mass Transfer 7 (1964), 681-694.
[18] Hadj Nacer M, Graur I, Perrier P, Méolans JG, Wuest M. Gas flow through microtubes with different internal surface coatings. J Vac Sci Technol A. 32 (2014) 021601.
[19] C. Aubert, and S. Colin, "High-order boundary conditions for gaseous flows in rectangular microchannels." Microscale Thermophysical Engineering 5,1 (2001), 41-54.

Appendix. INRIM and ICA results for each gas and different experimental set up.

	He							
	Δp Pa	p_i Pa	p_o Pa	T K	Kn_0	$q(T)$ mol s^{-1}	$u(q)$ mol s^{-1}	$u(q)/q$ %
Setup fig. 3	50	50	5.3E-08	293.5	1438	5.575E-11	9.5E-13	1.70
	50	50	5.3E-08	293.5	1440	5.588E-11	9.5E-13	1.70
	101	101	9.8E-08	293.5	714.9	1.100E-10	1.6E-12	1.50
	1002	1002	7.5E-07	293.5	72.24	9.339E-10	7.7E-12	0.82
	10011	10011	6.5E-06	293.5	7.229	7.181E-09	3.9E-11	0.54
	100881	100881	4.9E-05	293.5	0.717	6.035E-08	1.9E-10	0.32
Setup fig. 2	2201.9	100040	97838	293.1	0.366	2.262E-09	6.1E-11	2.70
	5192	103027	97835	293.1	0.360	3.703E-09	5.2E-11	1.40
	7178	105009	97831	293.1	0.357	4.584E-09	6.0E-11	1.30
	10212	108030	97818	293.1	0.351	6.068E-09	6.7E-11	1.10
	20220	118038	97818	293.1	0.335	1.176E-08	1.2E-10	1.00
	50110	147939	97829	293.1	0.294	2.984E-08	1.2E-10	0.40
	70320	168152	97832	293.1	0.272	4.160E-08	1.2E-10	0.30
	99695	197525	97830	293.1	0.245	5.952E-08	3.0E-10	0.50

Table A1

	Ar							
	Δp Pa	p_i Pa	p_o Pa	T K	Kn_0	$q(T)$ mol s^{-1}	$u(q)$ mol s^{-1}	$u(q)/q$ %
Setup fig. 3	50	50	4.3E-08	293.5	524.2	1.595E-11	3.7E-13	2.30
	101	101	8.2E-08	293.5	261.8	3.040E-11	5.5E-13	1.80
	1002	1002	6.5E-07	293.5	26.34	2.423E-10	2.7E-12	1.10
	10607	10607	4.7E-06	293.5	2.487	1.998E-09	1.4E-11	0.72
	100781	100781	5.1E-05	293.5	0.262	2.066E-08	8.3E-11	0.40
Setup fig. 2	2274	99419	97145	293.1	0.134	5.676E-10	1.5E-11	2.70
	5302	102461	97159	293.1	0.132	1.328E-09	1.9E-11	1.40
	7315	104562	97247	293.1	0.131	1.852E-09	2.2E-11	1.20
	10250	107529	97279	293.1	0.129	2.617E-09	2.1E-11	0.80
	20200	117500	97300	293.1	0.123	5.454E-09	5.5E-11	1.00
	50350	147663	97313	293.1	0.108	1.424E-08	8.5E-11	0.60
	69580	166899	97319	293.1	0.100	2.074E-08	6.2E-11	0.30
	99490	196810	97320	293.1	0.090	3.135E-08	6.3E-11	0.20
Setup fig. 4	992	1002	10	293.0	26.04	2.449E-10	9.8E-12	4.00
	10596	10607	11	292.5	2.480	2.050E-09	8.2E-11	4.00
	100757	100781	24	292.1	0.261	2.052E-08	8.2E-10	4.00
	6535	102798	96263	292.0	0.132	1.520E-09	6.1E-11	4.00
	7572	104876	97304	292.0	0.130	1.756E-09	7.0E-11	4.00
	9938	107238	97300	292.1	0.129	2.688E-09	1.1E-10	4.00
	20200	117716	97516	292.0	0.122	5.369E-09	2.1E-10	4.00

Table A2

	N_2							
	Δp Pa	p_i Pa	p_o Pa	T K	Kn_0	$q(T)$ mol s^{-1}	$u(q)$ mol s^{-1}	$u(q)/q$ %
Setup fig. 3	50	50	4.0E-08	293.5	488.7	1.847E-11	4.2E-13	2.30
	50	50	4.0E-08	293.5	488.9	1.854E-11	4.3E-13	2.30
	50	50	4.0E-08	293.5	488.7	1.849E-11	4.3E-13	2.30

	101	101	7.6E-08	293.5	243.4	3.573E-11	6.4E-13	1.80
	101	101	7.6E-08	293.5	243.4	3.574E-11	6.4E-13	1.80
	300	300	1.8E-07	293.5	81.74	9.770E-11	1.6E-12	1.60
	300	300	1.8E-07	293.6	81.75	9.761E-11	1.6E-12	1.60
	501	501	2.9E-07	293.6	49.02	1.546E-10	1.9E-12	1.20
	502	502	2.9E-07	293.6	48.94	1.548E-10	1.9E-12	1.20
	700	700	4.4E-07	293.6	35.05	2.086E-10	2.3E-12	1.10
	701	701	4.4E-07	293.6	35.04	2.086E-10	2.3E-12	1.10
	1000	1000	5.9E-07	293.6	24.54	2.861E-10	2.9E-12	1.00
	1001	1001	5.9E-07	293.6	24.53	2.863E-10	2.9E-12	1.00
	3004	3004	1.5E-06	293.7	8.173	7.587E-10	6.3E-12	0.83
	3005	3005	1.5E-06	293.7	8.169	7.582E-10	6.3E-12	0.83
	7013	7013	3.1E-06	293.7	3.501	1.619E-09	1.2E-11	0.75
	7003	7003	3.1E-06	293.7	3.506	1.617E-09	1.2E-11	0.75
	10014	10014	4.0E-06	293.7	2.452	2.239E-09	1.6E-11	0.71
	10014	10014	4.0E-06	293.7	2.452	2.239E-09	1.6E-11	0.71
	30327	30327	1.1E-05	293.7	0.810	6.499E-09	3.5E-11	0.54
	30323	30323	1.1E-05	293.7	0.810	6.498E-09	3.5E-11	0.54
	50037	50037	1.8E-05	293.7	0.491	1.101E-08	5.2E-11	0.47
	50031	50031	1.8E-05	293.7	0.491	1.103E-08	5.2E-11	0.47
	70162	70162	2.6E-05	293.7	0.350	1.617E-08	7.0E-11	0.43
	70203	70203	2.6E-05	293.7	0.350	1.621E-08	7.0E-11	0.43
	101719	101719	4.1E-05	293.8	0.241	2.540E-08	9.7E-11	0.38
	100724	100724	4.0E-05	293.8	0.244	2.514E-08	9.6E-11	0.38
	50	50	5.1E-06	293.6	488.0	1.810E-11	4.2E-13	2.30
	101	101	9.8E-06	293.6	243.8	3.535E-11	6.4E-13	1.80
	301	301	2.4E-05	293.6	81.67	9.713E-11	1.6E-12	1.60
	501	501	3.9E-05	293.6	49.02	1.552E-10	1.9E-12	1.20
	50	50	3.8E-06	293.6	493.3	1.782E-11	4.1E-13	2.30
	100	100	7.4E-06	293.6	244.6	3.508E-11	6.3E-13	1.80
	301	301	1.8E-05	293.6	81.67	9.709E-11	1.6E-12	1.60
Setup fig. 2	2048	100748	98700	293.1	0.123	6.733E-10	1.6E-11	2.40
	5052	103753	98701	293.1	0.121	1.670E-09	3.7E-11	2.20
	7085	105815	98730	293.1	0.120	2.234E-09	1.8E-11	0.80
	10039	108791	98752	293.1	0.118	3.201E-09	3.2E-11	1.00
	20100	118877	98777	293.1	0.113	6.625E-09	6.0E-11	0.90
	50130	148897	98767	293.1	0.099	1.764E-08	7.1E-11	0.40
	70065	168832	98767	293.1	0.092	2.563E-08	5.1E-11	0.20
	100080	198856	98776	293.1	0.082	3.884E-08	3.9E-11	0.10
	37175	137002	99827	293.1	0.104	1.279E-08	6.4E-11	0.50
	31665	131489	99824	293.1	0.106	1.071E-08	5.4E-11	0.50
	55050	154884	99834	293.1	0.096	1.960E-08	5.9E-11	0.30
	26190	126003	99813	293.1	0.109	8.761E-09	6.1E-11	0.70
	41700	141525	99825	293.1	0.102	1.443E-08	5.8E-11	0.40
Setup Fig. 4	100704	100724	20	292.3	0.243	2.503E-08	1.0E-09	4.00
	70187	70204	17	292.3	0.349	1.618E-08	6.5E-10	4.00
	50016	50031	15	292.3	0.489	1.094E-08	4.4E-10	4.00
	30309	30322	13	292.3	0.807	6.476E-09	2.6E-10	4.00
	10003	10014	11	292.3	2.443	2.234E-09	8.9E-11	4.00
	6993	7003	11	292.3	3.492	1.623E-09	6.5E-11	4.00
	2995	3005	10	292.3	8.123	7.424E-10	3.0E-11	4.00
	991	1001	10	292.3	24.24	2.936E-10	1.2E-11	4.00
	20101	118555	98454	292.3	0.113	6.815E-09	2.7E-10	4.00
	10502	109249	98747	292.3	0.118	3.415E-09	1.4E-10	4.00
	7068	105774	98707	292.3	0.120	2.385E-09	9.5E-11	4.00
	4969	101463	96494	292.3	0.124	1.680E-09	6.7E-11	4.00

Table A3

	N_2/H_2							
	Δp Pa	p_i Pa	p_o Pa	T K	Kn_0	$q(T)$ mol s^{-1}	$u(q)$ mol s^{-1}	$u(q)/q$ %
Setup fig. 2	2204	98981	96777	293.1	0.127	7.524E-10	2.3E-11	3.10
	5260	102030	96770	293.1	0.125	1.770E-09	2.3E-11	1.30
	7232	104001	96769	293.1	0.124	2.352E-09	3.1E-11	1.30
	10267	107031	96764	293.1	0.122	3.370E-09	2.4E-11	0.70
	20255	117009	96754	293.1	0.116	6.840E-09	6.2E-11	0.90
	50495	147248	96753	293.1	0.102	1.817E-08	7.3E-11	0.40
	70660	167409	96749	293.1	0.094	2.643E-08	7.9E-11	0.30
	100700	197434	96734	293.1	0.084	3.999E-08	8.0E-11	0.20

Table A4

	R12							
	Δp Pa	p_i Pa	p_o Pa	T K	Kn_0	$q(T)$ mol s^{-1}	$u(q)$ mol s^{-1}	$u(q)/q$ %
Setup fig. 2	2237	99267	97030	293.2	0.040	6.370E-10	3.1E-11	4.80
	5264	102304	97040	293.2	0.039	1.508E-09	2.7E-11	1.80
	7209	104247	97038	293.2	0.039	2.093E-09	4.6E-11	2.20
	10052	107156	97104	293.1	0.038	2.964E-09	1.9E-11	0.65
	20340	117477	97137	293.1	0.036	6.218E-09	4.4E-11	0.70
	50585	147736	97151	293.1	0.032	1.735E-08	1.0E-10	0.60
	70645	167803	97158	293.1	0.029	2.602E-08	1.0E-10	0.40
	100590	197783	97193	293.1	0.026	4.034E-08	4.0E-11	0.10

Table A5

	CO2							
	Δp Pa	p_i Pa	p_o Pa	T K	Kn_0	$q(T)$ mol s^{-1}	$u(q)$ mol s^{-1}	$u(q)/q$ %
Setup fig. 2	2268	99107	96839	293.2	0.083	6.699E-10	2.1E-11	3.10
	5260	102110	96850	293.2	0.082	1.616E-09	4.8E-11	3.00
	7390	104121	96731	293.2	0.081	2.402E-09	2.6E-11	1.10
	10323	107199	96876	293.2	0.080	3.166E-09	2.8E-11	0.90
	20245	117133	96888	293.2	0.076	6.656E-09	6.7E-11	1.00
	50450	147359	96909	293.2	0.067	1.753E-08	1.1E-10	0.60
	70555	167473	96918	293.2	0.062	2.585E-08	1.0E-10	0.40
	100350	197263	96913	293.2	0.056	3.920E-08	1.6E-10	0.40
Setupfig.4	19395	117198	97802	292.2	0.076	6.021E-09	2.4E-10	4.00
	10424	107348	96924	292.2	0.080	3.058E-09	1.2E-10	4.00
	19338	116796	97458	294.9	0.076	5.839E-09	2.3E-10	4.00
	17962	116351	98388	294.9	0.076	5.684E-09	2.3E-10	4.00
	7412	104304	96893	294.9	0.081	2.322E-09	9.3E-11	4.00

Table A6